Contrasting Nonaqueous against Aqueous Solvation on the Basis of Scaled-Particle Theory

Henry S. Ashbaugh*

Department of Chemical and Biomolecular Engineering, Tulane University, New Orleans, Louisiana 70118

Lawrence R. Pratt

Theoretical Division, Los Alamos National Laboratory, Los Alamos, New Mexico 87545

Received: March 11, 2007; In Final Form: May 25, 2007

Normal hexane is adopted as a typical organic solvent for comparison with liquid water in modern theories of hydrophobic hydration, and detailed results are worked-out here for the C-atom density in contact with a hard-sphere solute, $\rho_C G(R)$, for the full range of solute radii. The *intra*molecular structure of an *n*-hexane molecule introduces qualitative changes in $G(R)$ compared to scaled-particle models for liquid water. Also worked-out is a revised scaled-particle model implemented with molecular simulation results for liquid *n*-hexane. The classic scaled-particle model, acknowledging the intramolecular structure of an *n*-hexane molecule, is in qualitative agreement with the revised scaled-particle model results, and is consistent in sizing the methyl/methylene sites which compose *n*-hexane in the simulation model. The classic and revised scaled-particle models disagree for length scales greater than the radius of a methyl group, however. The liquid−vapor surface tension of *n*-hexane predicted by the classic scaled-particle model is too large, though the temperature variation is reasonable; this contrasts with the classic scaled-particle theory for water which predicts a reasonable magnitude of the water liquid−vapor surface tension, but an incorrect *sign* for the temperature derivative at moderate temperatures. Judging on the basis of the arbitrary condition that *drying* is indicated when $G(R) <$ 1, hard spheres dry at smaller sizes in *n*-hexane than in liquid water.

I. Introduction

Hydrophobic effects are foundational to aqueous phase nanotechnology, and biomolecular assembly and function. Scaled-particle approaches have provided the most effective framework for recent progress in understanding hydrophobic effects,[1,2] a framework with an extended history,[3−9] which contrasts sharply with traditional concepts of hydrophobic effects.[10−16] Important for understanding hydrophobic effects is a comparison between liquid water and organic solvents as media for solutes that do not express chemical or electrostatic interactions upon the solution. This paper presents results for such a comparison, adopting *n*-hexane as a typical organic solvent for the desired comparison.

In the context of classic applications of scaled-particle theory (SPT),[17] aqueous and nonaqueous solvents have been viewed as differing only on the basis of the size-parameter associated with hard-sphere packing, as opposed to intermolecular interactions more specifically.[3,18−20] A countervailing view[1,7,8,21] has been based on direct interrogation of spontaneous cavity formation in molecular simulations of water, *n*-hexane, *n*-decane, and polyethylene. In that argument alkanes are not treated simply as single hard spheres much larger than a water molecule, but as bonded collections of interaction sites, for example as methyl and methylene groups only slightly larger than a water molecule. To the extent that a molecularly detailed view is relevant, then the assertion that hydrophobic effects principally arise from molecular size differences is problematic. It has, indeed, been demonstrated that classic scaled-particle models unsatisfactorily represent the structure of organic liquids and the corresponding density fluctuations that give rise to cavity formation.[7,8] For the case of liquid water, which is more favorable for application of classic SPT, it was recognized long ago that some of the thermodynamic predictions are seriously erroneous.[2,4−6] It is argued in ref 21, contrary to the proposal of ref 18, that variability in H-bonding leads to multiple effective sizes of water molecules.

Applications of classic SPT[3] do have the drawback that the specific liquid structure assumed is parametrized solely by an empirical hard-sphere diameter for a solvent molecule. The application of expressions derived for the hard-sphere fluid to real liquids is questionable when the distinctions between specific molecular structures are of interest, as they are for organic solvents.

Considering liquid water along its vapor saturation curve, Stillinger extended SPT to treat explicitly the solvent structure quantified by known pair-correlations.[6] Furthermore, Stillinger embedded the experimentally known equation-of-state and liquid−vapor surface tension into the formulation which provides a more accurate description of cavity formation in aqueous solution. Following those ideas, a revised SPT was introduced in ref 2. That revision employed molecular simulations to provide multi-body correlations responsible for molecular sized cavity formation, using this framework to investigate the multiple scales of biomolecular hydration.

Presently, we address the roles of intra- and intermolecular correlations in cavity formation in *n*-hexane, contrasting hard-sphere solvation in aqueous and nonaqueous solution. Molecular simulations of *n*-hexane and water are performed to provide molecular correlation information that can be incorporated into a revised SPT framework. Though we follow the foundational

studies of Pohorille and Pratt,[7−9] the level of detail of *n*-hexane and water incorporated in the present modern SPT is unprecedented. This allows us to extend studies previously limited to molecular-sized hard spheres to meso- and macroscale surfaces. In addition we produce detailed thermodynamic properties, and address fundamental issues concerning the drying of extended surfaces.

II. Theoretical Development

An up-to-date review of scaled-particle theory approaches in this context appears in ref 2. The details are presented here only briefly.

The chemical potential of a mono-atomic solute, "A", can be expressed as

$$\mu_A(S) = kT \ln[\rho_A(S)\Lambda_A{}^3] + \mu_A^{ex}(S) \qquad (1)$$

Here *k* is Boltzmann's constant, *T* is the temperature, $\rho_A(S)$ is the solute number density in solution with solvent S, and Λ_A is the thermal de Broglie wavelength of the solute. μ_A^{ex} is the excess chemical potential, and is the target of the modeling here.

As it is the case for both water and *n*-hexane in the models treated here, we will assume that the polyatomic solvent molecules are composed of a single type of interaction site. This assumption can be relaxed, resulting in additional accounting of the varying diameters of the constituent solvent sites. We then introduce the bulk density of solvent sites, $\rho_\alpha = n_\alpha \times \rho_S$, the product of the number of solute interaction sites per molecule, n_α, and the solvent molecular density, ρ_S. Confining our discussion to impenetrable hard-sphere (HS) solutes, the solute excess chemical potential in solution is

$$\mu_A^{ex}(S) = -kT \ln p_0(R) \qquad (2)$$

where the insertion probability, $p_0(R)$, is the probability that a solute-sized stencil randomly placed in solution is devoid of solvent interaction centers.[2] The solvent accessible radius, *R*, is the distance of closest approach between the solute and solvent interaction centers, naturally taken as the sum of the van der Waals radius of a solvent interaction center and the radius of the HS solute, i.e., $R = (\sigma_{\alpha\alpha} + \sigma_{AA})/2$.

The relationship between the chemical potential and the solvent structure in the vicinity of the solute is

$$\delta\mu_A^{ex} = kT\, \rho_\alpha G(R)(4\pi R^2 \delta R) \qquad (3)$$

following directly from the potential distribution theorem.[22] The combination $\rho_\alpha G(R)$ is the density of solvent sites in contact with the HS solute. The desired excess chemical potential is then obtained by integrating this relationship

$$\mu_A^{ex}(S) = kT\, \rho_\alpha \int_0^R G(r)4\pi r^2 dr \qquad (4)$$

noting that $\mu_A^{ex}(S)$ vanishes when the interactions vanish. The product $kT\, \rho_\alpha G(R)$ has dimensions of force/area, and is the pressure due to solvent collisions with the hard surface of the solute. The chemical potential then is the quasi-static pressure−volume work required to expand the solute into solution. The relationship between the contact values and the insertion probability is

$$\rho_\alpha 4\pi R^2 G(R) = -\left(\frac{\partial \ln p_0(R)}{\partial R}\right) \qquad (5)$$

determined by differentiation of eq 4.

When the solute sphere is small enough, the *intra*molecular complexity of the polyatomic solvent molecule can be fully incorporated. When only one solvent molecule might fit within the cavity boundary, the insertion probability is

$$p_0(R \to 0) = 1 - \rho_S V_{exc}(R) \qquad (6)$$

where V_{exc} is the volume excluded to the solute by a single solvent molecule.[2] Though the shape of the excluded volume might be complicated, this is merely the fractional free volume in the case that the solute is so small that it never interacts with more than one solvent molecule at a time. The expression corresponding to eq 6 for the contact function is

$$\rho_\alpha 4\pi R^2 G(R \to 0) = \left(\frac{\rho_S}{1 - \rho_S V_{exc}(R)}\right)\frac{dV_{exc}(R)}{dR} \qquad (7)$$

This result is accurate in solvents with realistic interactions for a hard sphere radius up to $R \approx \sigma_{\alpha\alpha}/2$, and is exact for a HS solvent because the solute corresponds to a point particle with a van der Waals radius of zero. Larger HS solutes can contact more than one solvent molecule at a time, requiring information on multibody intermolecular correlations.

In the case that the solvent molecule is composed of a single spherical excluding site, $V_{exc}(R) = 4\pi R^3/3$, and eqs 6 and 7 reduce to

$$p_0(R \to 0) = 1 - 4\pi R^3 \rho_S/3 \qquad (8a)$$

$$G(R \to 0) = \frac{1}{1 - 4\pi R^3 \rho_S/3} \qquad (8b)$$

which are historical results.[23]

In the limit of a macroscopically large hard sphere, the contact values can be represented as an asymptotic expansion in $1/R$

$$G(R) \sim \sum_{j \geq 0} \frac{G_j}{R^j} \qquad (9)$$

Retaining contributions up to $j = 2$ yields[3,6,17,23,24]

$$kT\, \rho_\alpha G(R) \sim p_{sat} + \frac{2\gamma_\infty}{R} - \frac{4\gamma_\infty\delta}{R^2} \qquad (10)$$

where *p* is here to equal the liquid saturation pressure p_{sat}, γ_∞ is the surface tension of a flat interface, and δ[25] describes the initial curvature correction to the surface tension. The classic scaled-particle model is obtained by assuming that[3,6,17,23,24]

$$G(R) \sim \frac{\beta p_{sat}}{\rho_\alpha} + A\left(\frac{\sigma_{\alpha\alpha}}{2R}\right) + B\left(\frac{\sigma_{\alpha\alpha}}{2R}\right)^2 \qquad (11)$$

and determining the coefficients *A* and *B* so that this macroscopic form joins smoothly to the accurate result at the smallest scale, obtained from eq 7, at $R = \sigma_{\alpha\alpha}/2$.

Analytical formulas for the classic scaled-particle model are involved. We adopt the notation $V'_{exc} = dV_{exc}(R = \sigma_{\alpha\alpha}/2)/dR$, $V''_{exc} = d^2V_{exc}(R = \sigma_{\alpha\alpha}/2)/dR^2$, and $\eta = \rho_S V_{exc}(\sigma_{\alpha\alpha}/2)$ — the solvent packing fraction. Then

$$A = \frac{V''_{exc}}{n_\alpha 2\pi\sigma_{\alpha\alpha}(1-\eta)} + \frac{\rho_S[V'_{exc}]^2}{n_\alpha 2\pi\sigma_{\alpha\alpha}(1-\eta)^2} - 2\frac{\beta p_{sat}}{\rho_\alpha} \qquad (12)$$

$$B = \frac{V'_{\text{exc}}}{n_\alpha \pi \sigma_{\alpha\alpha}^2 (1 - \eta)} - \frac{V''_{\text{exc}}}{n_\alpha 2\pi \sigma_{\alpha\alpha}(1 - \eta)} -$$
$$\frac{\rho_S [V'_{\text{exc}}]^2}{n_\alpha 2\pi \sigma_{\alpha\alpha}(1 - \eta)^2} + \frac{\beta p_{\text{sat}}}{\rho \alpha} \quad (13)$$

Explicit formulas for $\beta\mu_A^{\text{ex}}$ can be obtained by integrating these results, namely

$$\frac{\mu_A^{\text{ex}}}{kT} =$$
$$\begin{cases} -\ln(1 - \rho_S V_{\text{exc}}(R)), & R \leq \sigma_{\alpha\alpha}/2 \\ -\ln(1 - \eta) + 3B\xi\left[\left(\frac{2R}{\sigma_{\alpha\alpha}}\right) - 1\right] \\ + \frac{3}{2}A\xi\left[\left(\frac{2R}{\sigma_{\alpha\alpha}}\right)^2 - 1\right] + \frac{\xi p_{\text{sat}}}{kT\rho_\alpha}\left[\left(\frac{2R}{\sigma_{\alpha\alpha}}\right)^3 - 1\right], & R > \sigma_{\alpha\alpha}/2 \end{cases}$$

$$(14)$$

where $\xi = \pi\rho_\alpha \sigma_{\alpha\alpha}^3/6$.

A more conclusive model was obtained in ref 2 by following Stillinger's suggestion[6] that solvent-specific information—both molecular correlations and macroscopic thermodynamic properties—be incorporated together into this chemical potential. Stillinger limited his information on correlations to the water oxygen−oxygen radial distribution. That information was augmented by ref 2 to include higher-order molecular correlations obtained from molecular simulations. An interpolation of the chemical potential between results for molecular length-scales from simulation, and the asymptotic macroscopic formula is

$$\mu_A^{\text{ex}}(R) = -kT \ln p_0(R)|_{\text{sim}} f(R) + \mu_A^{\text{ex}}(R)|_{\text{macro}} [1 - f(R)] \quad (15)$$

where $f(R)$ is a switching function parametrized to equal to one below R_{sim} and zero above R_{macro}, smoothly interpolating between these between these two limits. We use a cubic spline interpolating function, though other reasonable functions yield essentially indistinguishable predictions. The macroscopic chemical potential, determined by integration of the macroscopic cavity expression eq 10 is

$$\mu_A^{\text{ex}}(R)|_{\text{macro}} =$$
$$-\frac{4\pi kT \rho_W \lambda}{R} + \epsilon - 16\pi R\gamma_\infty\delta + 4\pi R^2 \gamma_\infty + \frac{4\pi}{3}R^3 p_{\text{sat}} \quad (16)$$

Rather than fitting the microscopic and macroscopic limits at a single point as in eqs 12 and 13, the parameters δ, λ, and integration constant ϵ are fitted to the simulation results between R_{sim} and R_{macro}. $G(R)$ is then determined by differentiation of the chemical potential (eq 3). An additional benefit of fitting eq 16 to the simulation insertion probabilities is that we do not have to numerically evaluate the first and second derivatives of the simulated insertion probabilities, which become more statistically uncertain with increasing cavity size. A related strategy for incorporating multibody correlations in $G(R)$ was suggested in ref 30.

III. Simulation Details

Molecular simulations were performed for liquid water and *n*-hexane from 270 to 370 K in 10 K increments along their experimental saturation curves. The simulations for water utilized standard Metropolis Monte Carlo procedures for a
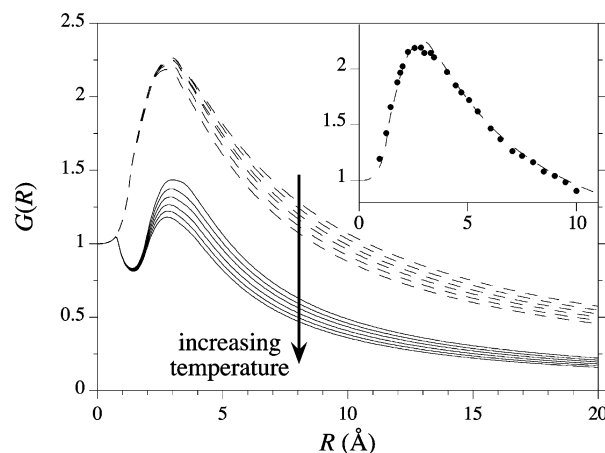

Figure 1. Contact values, $G(R)$, for hard spheres in water and *n*-hexane as determined from the revised scaled-particle model. Results for water are shown as dashed curves, while the results for *n*-hexane are shown as solid curves. Results are reported for temperatures of 270, 290, 310, 330, 350, and 370 K along the saturation curves of water and *n*-hexane. The inset compares predictions of $G(R)$ for liquid water at 300 K under the present approach to the MCNPT results[30] at 25 °C.

canonical ensemble; the use of Monte Carlo calculations here is for convenience, and should have no significance for our results. Bulk water was modeled using 268 SPC/E water molecules with periodic boundary conditions. Lennard-Jones potential interactions were smoothly truncated between water oxygen separations of 9.5 Å and 10 Å, while longer ranged electrostatic interactions were calculated using Ewald summation with conducting boundary conditions. After an equilibration phase of at least 10^5 MC passes, 5×10^6 MC production passes were carried out for analysis of thermodynamic averages. One pass corresponds to one attempted move per water molecule with 30% move acceptance. After every 50 MC passes, 10^5 particle insertions were attempted to determine averages for a total of 10^{10} insertions at each temperature. Statistical uncertainties were determined by grouping results into blocks of 10^6 MC passes.

Configurations of liquid *n*-hexane were generated using the molecular dynamics simulation package NAMD v2.5b3.40.[26,27] Bulk *n*-hexane was modeled using 216 molecules and the CHARMM19 united-atom potential[28] function within periodic boundary conditions. A carbon−carbon equilibrium bond length of 1.53 Å was used. Lennard-Jones potential interactions were evaluated smoothly truncating the potential based on the separation of *n*-hexane carbons between 9 Å and 10 Å. After an equilibration phase of at least 0.5 ns (using a 2 fs time step), 2 ns were carried out for analysis of thermodynamic averages. Every 0.4 ps, 4×10^5 particle insertions were attempted for a total of 2×10^9 insertions at each temperature. Statistical uncertainties were determined by grouping results into block averages over 0.4 ns each.

IV. Results and Discussion

The contact values for water and *n*-hexane as a function of temperature are shown in Figure 1. The magnitude of the contact values decrease with increasing temperature, and, as observed by Pratt and Pohorille[29] the contact values for *n*-hexane are lower than those for water. This is consistent with the idea that water squeezes more strongly on the HS surface driving nonpolar solutes into the organic phase. A distinctive characteristic of the *n*-hexane contact values is the kink at $R = 0.765$ Å, half the carbon−carbon bond length. This cusp results from the rigid overlap between exclusion-spheres centered on neighboring

Contrasting Nonaqueous against Aqueous Solvation

J. Phys. Chem. B, Vol. 111, No. 31, 2007 **9333**

bonded carbons and is further discussed below. For both water and n-hexane, $G(R)$ decreases with increasing solute radius, and eventually the contact density is less than the bulk liquid density. This dewetting occurs at smaller sizes for n-hexane than for water: $G(R)$ falls below one at $R \approx 5$ Å for n-hexane compared to $R \approx 10$ Å for water.

IV.A. Classic SPT for Water. The case of liquid water has been discussed in detail elsewhere,[2] but Figure 1 summarizes those results. The inset to Figure 1 compares the contact values from Monte Carlo NPT simulations of TIP4P water at 25C, 1 atm pressure recently reported by Floris[30] with our predictions using the revised SPT theory. The quantitative comparison is excellent, and it gives confidence that this revised SPT provides accurate predictions of the free energies of cavity formation. Important points for the subsequent discussion are that the classic SPT predictions are qualitatively reasonable, but the quantitative agreement is imperfect even if an effective $\sigma_{\alpha\alpha}$ is treated as an empirical function of T.[2,31] Classic SPT predicts that the maximum in $G(R)$ is shifted inward to $R_{max} \approx 2$ Å, while the true maximum is closer to 3 Å. Water has an open structure favoring larger cavities under these conditions. The resulting maximum in the pressure therefore is shifted out to larger radii.

IV.B. Classic SPT for n-Hexane. As a preliminary step, we first examine the origin of the cusp in $G(R)$ observed in Figure 1. This feature would be absent under the assumption that n-hexane is a hard sphere. As a result, free energy predictions of HS solvation free energies in n-hexane made using this assumption are ad hoc.[20,32] More seriously, this discontinuity in the slope of $G(R)$ rules-out a smooth interpolation of macroscopic results to the formula valid in the domain of R smaller than this break. The HS excluded volume for n-hexane can be expressed as

$$V_{exc}(R) = V_{exc}^{(1)}(R) + V_{exc}^{(2)}(R) + V_{exc}^{(3)}(R) + ... \qquad (17)$$

The contribution from exclusion-spheres individually, each an interaction site of n-hexane, is

$$V_{exc}^{(1)}(R) = \frac{4\pi R^3}{3} n_\alpha \qquad (18)$$

$V_{exc}^{(2)}(R)$ constitutes the reduction in the n-hexane excluded volume as a result of overlaps between bonded carbon sites. The principal contribution to $V_{exc}^{(2)}(r)$ is

$$V_{exc}^{(2)}(R) = \begin{cases} 0, & R \leq l/2, \\ -\frac{4\pi}{3}(n_\alpha - 1)\left(R^3 - \frac{3l}{4}R^2 + \frac{l^3}{16}\right), & R > l/2, \end{cases} \qquad (19)$$

where $l = 1.53$ Å is the carbon−carbon bond length. This contribution accounts for the observed cusp at $l/2 \approx 0.765$ Å. Another such contribution, with characteristic length $\sqrt{2/3} \times l \approx 1.25$ Å should be anticipated for 1−3 carbon overlaps. But that contribution is nearly exactly cancelled by a piece of $V_{exc}^{(3)}(R)$ which constitutes the change in the excluded volume as a result of overlaps between three contiguous bonded carbons. Thus, no cusp appears at 1.25 Å, though the approximation obtained by eqs 18 and 19 begins to deviate from the exact answer at this point (Figure 2). Analytical formulas for $V_{exc}^{(3)}(R)$ and its derivatives are more involved,[33] and, in view of these cancellations, augmentations of eqs 18 and 19 were evaluated numerically using MC integration. Contributions from $V_{exc}^{(n)}(R)$, for $n \geq 4$, are small and less singular. Contributions up to

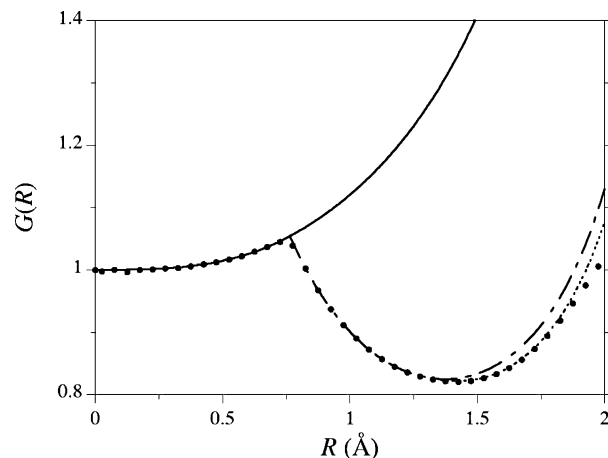**Figure 2.** Detail of the contact values for n-hexane at 300 K for small R. The points indicate simulation results. The curves indicate the predictions of eq 7 with contributions from $V_{exc}^{(1)}(r)$ (solid), eqs 18 and 19 (long−short dash), and up to $V_{exc}^{(3)}(r)$ (dotted).
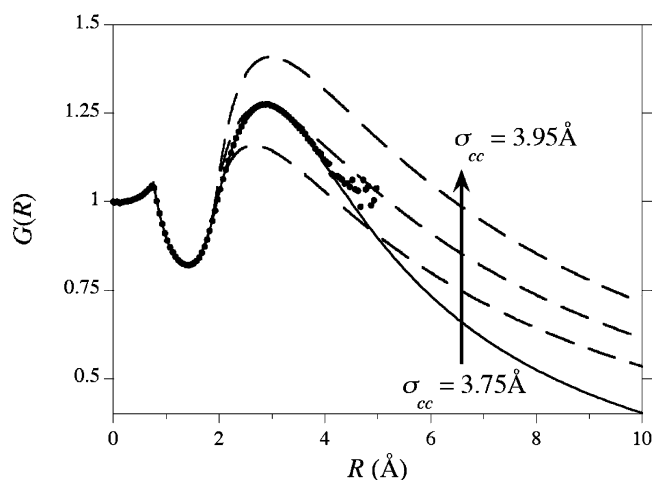

Figure 3. Hard sphere contact values for n-hexane at 300 K at liquid saturation. The points are obtained by differentiation of the insertion probabilities. The dashed lines are obtained from the classic SPT predictions for a HS solvent (eqs 7 and 11) using effective $CH_{2/3}$ HS diameters between $\sigma_{CC} = 3.75$ and 3.95 Å in 0.1 Å increments. The solid line is obtained by differentiation of the revised SPT, eq 15, fitted to the simulation results between $R_{sim} = 3.0$ Å and $R_{macro} = 4.5$ Å.

$V_{exc}^{(3)}(R)$ provides an accurate description of $G(R)$ up to $R \approx 1.9$ Å, at which point intermolecular correlations begin to contribute.

The classic SPT predictions for the contact values for n-hexane at 300 K (eqs 7 and 11) are in good qualitative agreement with the simulation and revised SPT results for molecularly sized cavities (Figure 3). In addition to reproducing the cusp, classic SPT correctly predicts the location and magnitude of the maximum at $R \approx 3$ Å using a physically reasonable $CH_{2/3}$ diameter of $\sigma_{CC} = 3.85$ Å. The agreement of classic SPT with simulation and the revised SPT predictions, however, breaks down for radii greater than 4 Å, beyond which classic SPT predicts a value larger than $G(R)$. It is heartening to observe that when the structure of solvent molecules is taken into account a more physically realistic $CH_{2/3}$ diameter of 3.85 Å is found, rather than an empirical diameter between 5.45 and 6.2 Å, depending on the solvation property being described, for an n-hexane molecule.[4,32,34,35]

Classic SPT provides a relationship for the surface tension of a flat interface. Comparing eqs 10−13 yields

9334 *J. Phys. Chem. B, Vol. 111, No. 31, 2007*

Ashbaugh and Pratt

$$\gamma_\infty = \left(\frac{kT\,\rho_S\sigma_{\alpha\alpha}}{8\pi}\right)\left\{\frac{V''_{exc}}{\sigma_{\alpha\alpha}(1-\eta)} + \frac{\rho_S[V'_{exc}]^2}{\sigma_{\alpha\alpha}(1-\eta)^2} - 4\pi\frac{\beta p_{sat}}{\rho_S}\right\} \quad (20)$$

The classic SPT predictions for the macroscopic surface tension of water and *n*-hexane are compared to the experimental liquid−vapor surface tension in Figure 4. While the magnitude of the aqueous surface tension determined by classic SPT is comparable to experiment, the predicted temperature dependence of the surface tension is incorrect.[4,6]

The predicted temperature dependence of the surface tension of *n*-hexane is in better qualitative agreement with the experimental trend (Figure 4). Both surface tensions decrease with increasing temperature by a comparable amount. The magnitude of the predicted surface tension, however, is approximately twice the experimental value. This difference is reflected in the slower predicted rate of decrease of $G(R)$ with increasing R compared to that determined from the experimental surface tension and the revised SPT prediction (Figure 3).

The thermodynamics of molecularly sized hard spheres in water and *n*-hexane at 300 K differ characteristically (Figure 5). To decompose the chemical potential into its entropic and enthalpic components, we assume that the heat capacity $c_A^{ex}(T_0)$ $= -T\partial s_A^{ex}/\partial T|_{sat}$ is independent of T. Under this satisfactory assumption

$$h_A^{ex} = h_A^{ex}(T_0) + (T - T_0)c_A^{ex}(T_0) \quad (21)$$

$$s_A^{ex} = s_A^{ex}(T_0) + \ln\left(\frac{T}{T_0}\right)c_A^{ex}(T_0) \quad (22)$$

and

$$\mu_A^{ex} = \mu_A^{ex}(T_0) + (T - T_0)(c_A^{ex}(T_0) - s_A^{ex}(T_0)) -$$
$$T\ln\left(\frac{T}{T_0}\right)c_A^{ex}(T_0) \quad (23)$$

The most distinctive difference between solvation in water and *n*-hexane is that the hydration of molecularly sized solutes is entropically unfavorable, whereas in *n*-hexane, solvation is only mildly opposed by entropy for small spheres ($R \approx 2$ Å) and favored by entropy for larger sizes. In *n*-hexane, moreover, HS solvation is predominantly opposed by enthalpy, while in water up to methane-sized spheres ($R = 3.3$ Å), enthalpy plays only a minor role in the overall hydration thermodynamics. We note that the simulation study of ref 32 found that HS solvation in both water and *n*-hexane is dominantly opposed by entropy, while energy plays little role in the HS thermodynamics. That study, however, considered the energy and enthalpy to be determined from the derivative of the chemical potential at constant volume, as opposed to along the saturation curve (indistinguishable from the constant pressure derivative at low pressures) as experimental measurements are typically performed and as considered here. The difference between these two partial derivatives is significant and accounts for the observed changes in the contributions of entropy and enthalpy.

Considered further in Figure 6 are the differences between aqueous and *n*-hexane solvation, illustrating how thermodynamic properties change with temperature. The chemical potential of the methane-sized hard sphere in water increases over this temperature range, indicative of an unfavorable entropy of hydration, while the opposite is true for *n*-hexane solvation. The HS solvation heat capacity in water is 232 J/(mol K), in excellent agreement with the experimental values for heat capacity between 209 and 237 J/(mol K) for methane at 298K;[2,36−38]
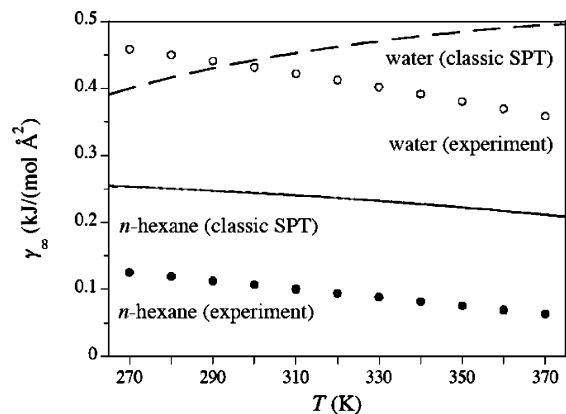

Figure 4. Surface tension of the flat liquid-cavity interface of water and *n*-hexane as a function of temperature along the saturation curve. Diameters for water and an *n*-hexane methyl/methylene units of $\sigma_{\alpha\alpha} = 2.8$ and 3.85 Å, respectively, were assumed.
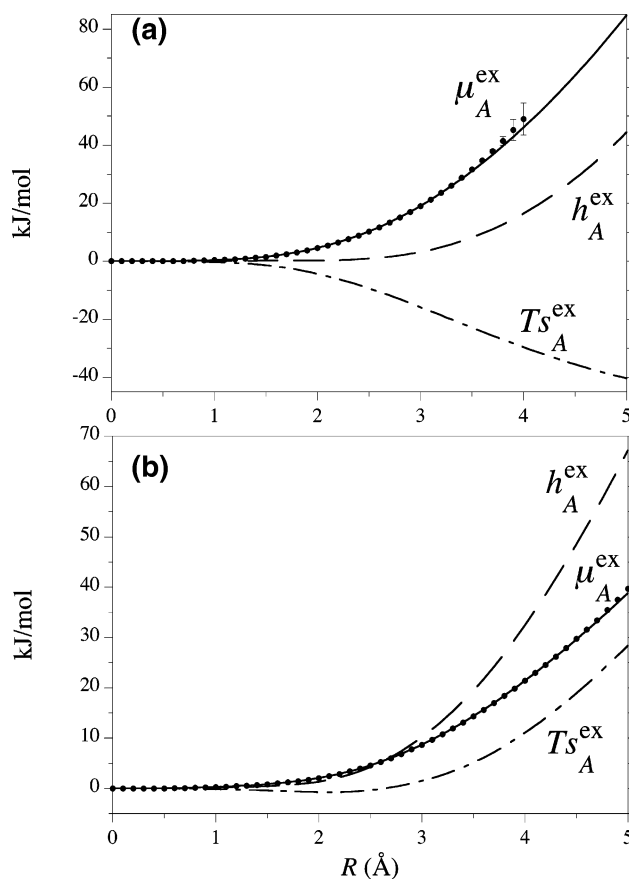

Figure 5. (a) Hard sphere solvation thermodynamics in water at 300 K at the saturation density. The points correspond to HS insertion results. Error bars correspond to 95% confidence limits. The solid, long dashed, and long−short dashed lines correspond to μ_A^{ex}, h_A^{ex}, and Ts_A^{ex}, respectively, determined by fitting eqs 22 and 23 to the revised scaled-particle model predictions. (b) As above but for *n*-hexane. In this case the 95% confidence limits are comparable to the size of the points.

the comparable value for *n*-hexane is 37 J/(mol K). These differences emphasize the larger temperature dependence of the HS entropy and enthalpy in water. While experiments have demonstrated that $c_A^{ex}(T_0)$ is small in organic solvents, accurate values are difficult to obtain. A range of 0−42 J/(mol K) for many organic solvents can estimated.[30] While the enthalpy of *n*-hexane solvation is positive over the entire temperature range, the hydration enthalpy changes sign between 270 and 280 K from negative to positive. A consequence of this sign change
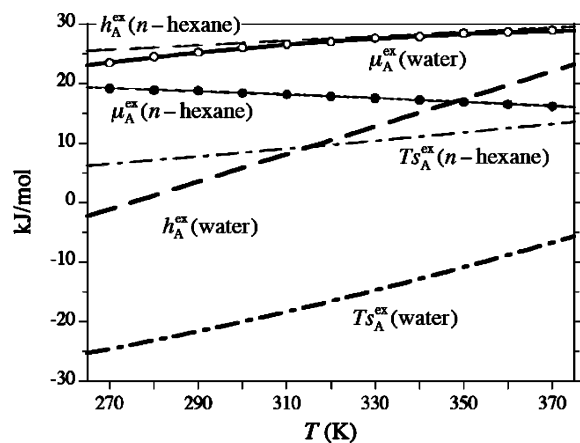
Contrasting Nonaqueous against Aqueous Solvation

J. Phys. Chem. B, Vol. 111, No. 31, 2007 **9335**

Figure 6. Solvation thermodynamics for a methane-sized HS in water ($R = 3.3$ Å) and *n*-hexane ($R = 3.8$ Å) as a function of temperature along the liquid saturation curve. The open and closed circles correspond to the simulation results for the chemical potential for water and *n*-hexane, respectively. Error bars are smaller than the symbols. The solid, long dashed, and long−short dashed lines correspond to μ_A^{ex}, h_A^{ex}, and Ts_A^{ex}, respectively, determined by fitting eq 20 to the revised scaled-particle model predictions. The thick and thin lines denote results for water and *n*-hexane, respectively.

is that the HS solubility exhibits a minimum at the point at which the enthalpy is zero. This behavior has been previously tied to the temperature of maximum density of liquid water at 277 K.[2,40,41]

The SPT approach systematically interpolates the surface tension between molecular and macroscopic length scales. Under the assumption that the pressure contribution to the solvation free energy is negligible, an excellent assumption for liquids at ambient pressures, the surface tension for solvating a HS solute is determined by the surface area derivative of the chemical potential with respect to the HS surface area. This derivative depends on the definition of the solute surface area,[2,42] but here we restrict consideration to the area of the spherical solute excluded volume of radius R. Differentiating the chemical potential with respect to this surface area yields

$$\gamma(R) = \frac{\partial \mu_A^{ex}}{\partial 4\pi R^2} = \frac{1}{2} kT\rho_\alpha G(R)R \tag{24}$$

The molecular surface tension of water and *n*-hexane as a function of R at 300 K is shown in Figure 7. For small hard spheres, all the surface thermodynamic properties go to zero as $R \rightarrow 0$. With increasing size, the molecular surface tension of water increases monotonically and approaches towards its asymptotic limit for a flat interface, $\gamma_\infty = 0.432$ kJ/(mol Å²) = 71.7 dyn/cm for water. For methane sized hard spheres, the molecular surface tension is only about half the macroscopic value. The molecular surface tension surface tension of *n*-hexane slightly overshoots its plateau value and passes through a maximum at sizes comparable to a CH_n site, and then asymptotically decays to the flat interface value, $\gamma_\infty = 0.107$ kJ/(mol Å²) = 17.8 dyn/cm, with increasing size. The asymptotic approach to the macroscopic limit is slower for water than for *n*-hexane.

Examination of the surface entropy is interesting. The surface entropy in water is initially negative but becomes positive for spheres greater than $R \approx 6$ Å. The HS solvation entropy in *n*-hexane is different. While the surface entropy is negative for spheres less than ≈2.5 Å in radius, this size is a lower limit for solutes of practical interest. For molecularly sized hard spheres
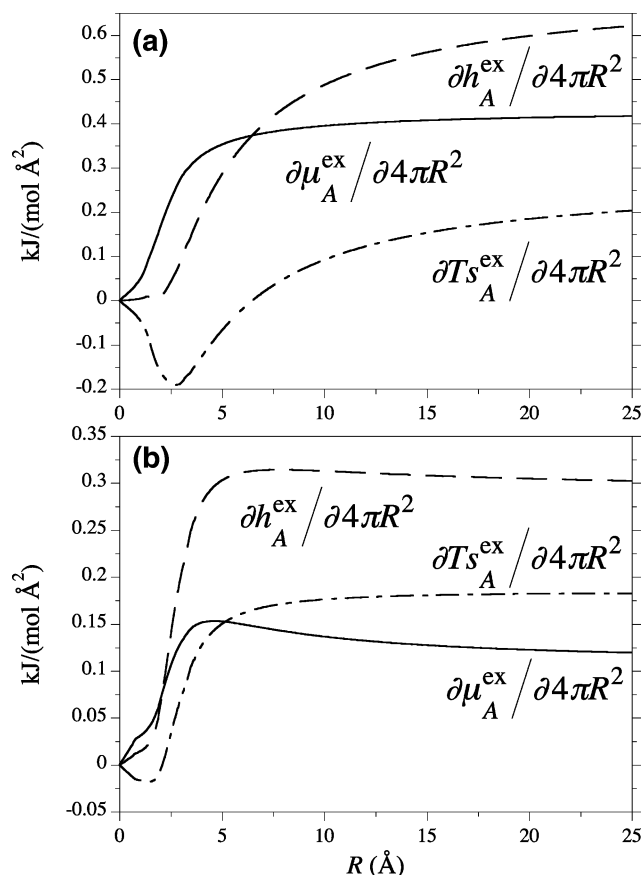

Figure 7. (a) Derivative of μ_A^{ex}, h_A^{ex}, and Ts_A^{ex} with respect to the HS surface area, $A = 4\pi R^2$, in water at 300 K as a function of the HS size from molecular to mesoscopic surfaces. The solid, long dashed, and long−short dashed lines correspond to μ_A^{ex}, h_A^{ex}, and Ts_A^{ex}, respectively, determined by fitting eqs 22 and 23 to the revised SPT predictions. (b) As above but for *n*-hexane.

though, the surface entropy rapidly approaches that of a macroscopic interface.

While the surface enthalpy for both water and *n*-hexane is positive at 300 K, the enthalpy in water more slowly approaches the macroscopic-surface value than does the surface free energy, whereas the enthalpy in hexane appears to approach the macroscopic asymptote more quickly than does the surface free energy. These observations indicate that solvation properties in water are expected to vary more importantly with solute size than in *n*-hexane.

V. Concluding Discussion

The intramolecular structure of *n*-hexane can be incorporated into a generalization of classic scaled-particle models of solvation of inert gases in that solvent. That generalization accesses a length-scale that is suitable for interpolation between macroscopic and *n*-hexane intramolecular lengths. Thus, atomic-scale resolution is essential for formulating and implementing accurate scaled-particle models for HS solvation in organic solvents. Judging on the basis of the arbitrary condition that *drying* is indicated when $G(R) < 1$, hard-sphere solutes reach drying conditions at smaller sizes for *n*-hexane than they do for liquid water. Factors other than proximity to a vapor−liquid coexistence point, for example molecular-scale surface roughness,[43] can reduce the contact value $G(R)$. Nevertheless, it is a direct and primitive indication of hydrophobicity that $G(R)$ is greater for the case of liquid water than for *n*-hexane (Figure

1); liquid water squeezes-out hard spherical solutes more forcefully than does *n*-hexane.

The initial success of application of classic SPT to hydrophobic hydration[3] immediately suggested[5] "an almost thermodynamic independence of molecular structure." Those successes were widely viewed as fortuitous,[6] because of the general expectation that the thermodynamic peculiarities of hydrophobic hydration should be explained on the basis of specific molecular structures characteristic of liquid water. The line of research into which this contribution fits eventually suggests a broader view, namely, that these thermodynamic peculiarities depend predominantly on generic features of aqueous solutions such as the equation-of-state.[44–46] This is supported by the well-known observation that the sum of the standard hydration entropies of $K^+(aq)$ and $Cl^-(aq)$ is about *twice* the standard hydration entropy of $Ar(aq)$,[47] whereas the case of methanol as a solvent is qualitatively different. The SPT then helpfully suggests the solvent *volume-change* as the structural coordinate most directly responsible for the thermodynamic peculiarities of hydrophobic hydration.[16,18,48] Of course, the equation of state of liquid water depends on interactions and structures of many types and at many length-scales.

A further conclusion, also supported by the work of ref 2, is that scaled-particle approaches can systematically and constructively include specific intra- and intermolecular structural characteristics of the solvent. Properly included, those structural features display clear distinctions from the classic scaled-particle theories.

References and Notes

(1) Pratt, L. R. *Annu. Rev. Phys. Chem.* **2002**, *53*, 409–436.
(2) Ashbaugh, H. S.; Pratt, L. R. *Rev. Mod. Phys.* **2006**, *78*, 159.
(3) Pierotti, R. A. *Chem. Rev.* **1976**, *76*, 717.
(4) Mayer, S. W. *J. Phys. Chem.* **1963**, *67*, 2160–2664.
(5) Ben-Naim, A.; Friedman, H. L. *Phys. J. Chem.* **1967**, *71*, 448.
(6) Stillinger, F. H. *J. Solution Chem.* **1973**, *2*, 141–158.
(7) Pohorille, A.; Pratt, L. R. *J. Am. Chem. Soc.* **1990**, *112*, 5066–5074.
(8) Pratt, L. R.; Pohorille, A. *Proc. Natl. Acad. Sci. U.S.A.* **1992**, *89*, 2995.
(9) Pratt, L. R.; Pohorille, A. In *Proceedings of the EBSA 1992 International Workshop on Water-Biomolecule Interactions*; Palma, M. U., Palma-Vittorelli, M. B., Parak, F., Eds.; Societá Italiana di Fisica: Bologna, Italy, 1993; p 261.
(10) Frank, H. S.; Evans, M. W. *J. Chem. Phys.* **1945**, *13*, 507.
(11) Tanford, C. *Protein Sci.* **1997**, *6*, 1358–1366.
(12) Scheraga, H. A. *J. Biomol. Struct. Dyn.* **1998**, *16*, 447–460.
(13) Muller, N. *Acc. Chem. Res.* **1990**, *23*, 23–28.
(14) Henn, A. R.; Kauzmann, W. *J. Phys. Chem.* **1989**, *93*, 3770–3783.
(15) Sharp, K. A.; Madan, B. *J. Phys. Chem. B* **1997**, *101*, 4343–4348.
(16) Lazaridis, T. *Acc. Chem. Res.* **2001**, *34*, 931–937.
(17) Reiss, H. *Adv. Chem. Phys.* **1965**, *9*, 1–84.
(18) Lee, B. *Biopolymers* **1985**, *24*, 813–823.
(19) Tomas-Oliveira, I.; Wodak, S. *J. Chem. Phys.* **1999**, *111*, 8576–8587.
(20) Graziano, G. *Biophys. Chem.* **2003**, *104*, 393–405.
(21) Garde, S.; Hummer, G.; Khare, R. *Polym. Mater.: Sci. Eng.* **2001**, *85*, (449)
(22) Beck, T. L.; Paulaitis, M. E.; Pratt, L. R. *The Potential Distribution Theorem and Models of Molecular Solutions*; Cambridge University Press: New York, 2006.
(23) Reiss, H. In *Statistical Mechanics and Statistical Methods in Theory and Application*; Landman, U., Ed.; Plenum: New York, 1977; pp 99–138.
(24) Henderson, J. R. *J. Chem. Phys.* **2002**, *116*, 5039–5045.
(25) Tolman, R. C. *J. Chem. Phys.* **1949**, *17*, 333–337.
(26) Kale, L.; Skeel, R.; Bhandarkar, M.; Brunner, R.; Gursoy, A.; Krawetz, N.; Phillips, J.; Shinozaki, A.; Varadarajan, K.; Schulten, K. *J. Comp. Phys.* **1999**, *151*, 283–312.
(27) Phillips, J. C.; Braun, R.; Wang, W.; Gumbart, J.; Tajkhorshid, E.; Villa, E.; Chipot, C.; Skeel, R. D.; Kale, L.; Schulten, K. *J. Comp. Chem.* **2005**, *26*, 1781–802.
(28) Brooks, B. R.; Bruccoleri, R. E.; Olafson, B. D.; States, D. J.; Swaminathan, S.; Karplus, M. *J. Comp. Chem.* **1983**, *4*, 187–217.
(29) Pratt, L. R.; Pohorille, A. *Proc. Natl. Acad. Sci. U.S.A.* **1992**, *89*, 2995–2999.
(30) Floris, F. M. *J. Phys. Chem. B* **2005**, *109*, 24061–24070.
(31) Graziano, G. *Chem. Phys. Letts.* **2006**, *432*, 84–87.
(32) Tomas-Oliveira, I.; Wodak, S. J. *J. Chem. Phys.* **1999**, *111*, 8576–87.
(33) Rowlinson, J. S. *Mol. Phys.* **1963**, *6*, 517–524.
(34) Graziano, G. *Biophys. Chem.* **2003**, *105*, 371–382.
(35) Kodaka, M. *J. Phys. Chem. B* **2001**, *105*, 5592–5594.
(36) Ben-Naim, A.; Marcus, Y. *J. Chem. Phys.* **1984**, *80*, 4438–40.
(37) Gill, S. J.; Dec, S. F.; Olofsson, G.; Wadso, I. *J. Phys. Chem.* **1985**, *89*, 3758–61.
(38) Naghibi, H.; Dec, S. F.; Gill, S. J. *J. Phys. Chem.* **1986**, *90*, 4621–4623.
(39) Eley, D. D. *Trans. Faraday Soc.* **1939**, *35*, 1421.
(40) Garde, S.; García, A. E.; Pratt, L. R.; Hummer, G. *Biophys. Chem.* **1999**, *78*, 21–32.
(41) Ashbaugh, H. S.; Truskett, T. M.; Debenedetti, P. G. *J. Chem. Phys.* **2002**, *116*, 2907–21.
(42) Ashbaugh, H. S.; Paulaitis, M. E. *J. Am. Chem. Soc.* **2001**, *123*, 10721–10728.
(43) Ashbaugh, H. S.; Pratt, L. R.; Paulaitis, M. E.; Clohecy, J.; Beck, T. L. *J. Am. Chem. Soc.* **2005**, *127*, 2808–2809.
(44) Pratt, L. R.; Pohorille, A. *Chem. Rev.* **2002**, *102*, 2671–2691.
(45) Pratt, L. R.; Pohorille, A.; Asthagiri, D. *What is Special About Water as a Matrix of Life*?; Los Alamos National Laboratory Technical Report LA-UR-05-3081; Los Alamos National Laboratory: Los Alamos, NM, 2005.
(46) Paschek, D. *J. Chem. Phys.* **2004**, *120*, 6674–90.
(47) Friedman, H. L.; Krishnan, C. V. In *Water A Comprehensive Treatise*; Franks, F., Ed.; Plenum: New York, 1973; Vol. 3, pp 1–118.
(48) Silverstein, T. P. *J. Chem. Ed.* **1998**, *75*, 116–118.